

Enhanced spontaneous emission in a photonic-crystal light-emitting diode

M. Francardi,^{1,a)} L. Balet,^{2,3} A. Gerardino,¹ N. Chauvin,² D. Bitauld,² L. H. Li,³ B. Alloing,³ and A. Fiore²

¹Institute for Photonics and Nanotechnologies-CNR, via Cineto Romano 42, 00156 Roma, Italy

²COBRA Research Institute, Eindhoven University of Technology, P.O. Box 513, 5600MB Eindhoven, The Netherlands

³Ecole Polytechnique Fédérale de Lausanne (EPFL), Institute of Photonics and Quantum Electronics, CH-1015 Lausanne, Switzerland

(Received 19 May 2008; accepted 2 July 2008; published online 6 October 2008)

We report direct evidence of enhanced spontaneous emission in a photonic-crystal (PhC) light-emitting diode. The device consists of *p-i-n* heterojunction embedded in a suspended membrane, comprising a layer of self-assembled quantum dots. Current is injected laterally from the periphery to the center of the PhC. A well-isolated emission peak at 1.3 μm from the PhC cavity mode is observed, and the enhancement of the spontaneous emission rate is clearly evidenced by time-resolved electroluminescence measurements, showing that our diode switches off in a time shorter than the bulk radiative and nonradiative lifetimes. © 2008 American Institute of Physics.

[DOI: [10.1063/1.2964186](https://doi.org/10.1063/1.2964186)]

Spontaneous emission results from the coupling of a quantum emitter to the surrounding electromagnetic environment. It therefore depends both on the emitter's dipole moment and on the density and properties of the available electromagnetic modes.¹ In particular, a wavelength-scale, low-loss cavity can provide an increase of spontaneous emission rate by a factor $\propto Q/V$ (Q , quality factor; V , mode volume) over the free-space value. This effect can be used to change the emission rate and at the same time efficiently funnel most of the spontaneously-emitted photons into a single well-controlled output mode, resulting in high extraction efficiency. After the first demonstration of enhanced spontaneous emission from quantum dots (QDs) in monolithic micropillars,² the control of spontaneous emission has been demonstrated with several types of cavities, under optical pumping. For practical applications, electrical pumping is needed. However, the implementation of electrical injection in a low-loss ultrasmall cavity requires the integration of electrical contacts in a micrometer-scale device and a careful control of device parasitics [to allow ultrafast (subnanosecond) electrical probing]. Indirect evidence of spontaneous emission control in electroluminescence (EL) has been recently deduced from the static characteristics of metallic-coated nanolasers³ and of electrically contacted micropillars.⁴ In this paper, we report a high-frequency photonic-crystal (PhC) light-emitting diode (LED) structure which allows the direct experimental measurement of cavity-enhanced spontaneous emission dynamics in a LED. Furthermore, the emission wavelength is around 1.3 μm , corresponding to a transmission window of optical fibers.

Our device (Fig. 1) consists of a membrane PhC cavity containing a *p-i-n* heterojunction, where holes are injected from a top ring *p*-contact and electrons from the sides of the mesa, using highly doped GaAs contact layers to spread the current throughout the mesa to the center of the cavity. As compared to injection through a central post,⁶ this approach allows an easier fabrication, and the decoupling of the prob-

lems of electrical injection and optimization of quality factor. Additionally, in contrast to previous approaches to PhC membrane LEDs,^{5,6} we are able to electrically address a single PhC cavity with low parasitic resistance and capacitance, allowing the fast electrical control needed for the time-resolved (IR) measurement of the emission dynamics.

The heterostructure used to fabricate the LEDs is grown by molecular beam epitaxy on a GaAs substrate and consists of a 370-nm-thick GaAs/Al_{0.2}Ga_{0.8}As *p-i-n* junction on the top of a 1500-nm-thick Al_{0.7}Ga_{0.3}As sacrificial layer. A single layer of low-density InAs QDs (5–7 dots/ μm^2) emitting at 1300 nm at 5 K is grown using a very low InAs deposition rate $\approx 2 \times 10^{-3}$ ML/s.⁷ The fabrication process is based on several e-beam lithography steps and typical thin-film processes. We first define 8 μm diameter, 320-nm-deep circular mesas by wet etching down to the bottom *n*-contact layer. Then, a ring-shaped *n*-contact is defined by lift-off of a 155-nm-thick Ni/Ge/Au/Ni/Au multilayer that is subsequently annealed at 400 °C for 30 min. A 200-nm-thick Si₃N₄ layer is deposited to isolate the *n* and *p* contacts and then removed from the *n*-contact and from the top of the mesa. By lift-off of a 110-nm-thick Cr/Au bilayer, we realize an annular *p*-contact on the top of the mesa. In the same evaporation step, the top *p*-contact and the bottom *n*-contact are connected to ground-signal-ground coplanar electrodes on the top of the Si₃N₄ surface. An annular gold cover is

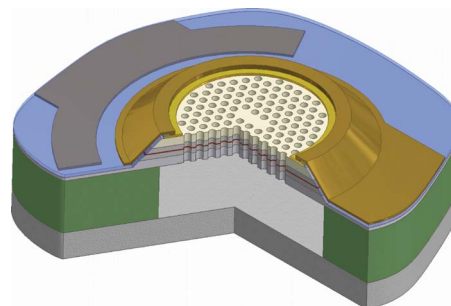


FIG. 1. (Color online) Sketch of the LED showing the *p-i-n* heterojunction suspended membrane.

^{a)}Electronic mail: marco.francardi@ifn.cnr.it.

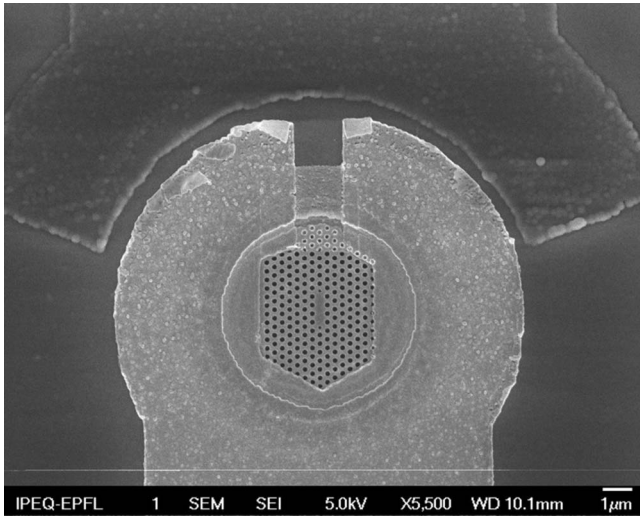


FIG. 2. SEM of a 8 μm diameter PhC LED. The p -contact is clearly visible on the bottom side, whereas the n -contact is shaded by the Si_3N_4 insulating layer.

evaporated around the entire mesa edge in order to filter out light scattered by the mesa sidewalls. A 150-nm-thick SiO_2 layer is then deposited and the PhC pattern—aligned to the mesa—is defined on a 200-nm-thick resist and transferred to the SiO_2 layer and then to the GaAs/AlGaAs membrane ($\text{SiCl}_4/\text{O}_2/\text{Ar}$ based reactive ion etching). Finally, the bottom $\text{Al}_{0.7}\text{Ga}_{0.3}\text{As}$ layer sacrificial layer is selectively removed using a diluted HF solution. A scanning-electron microscope (SEM) image of the LED at the end of the fabrication process is shown in Fig. 2. The PhC nanocavities that have been integrated with the LED are L3 modified nanocavities,^{1,8} characterized by a triangular lattice with a fixed filling factor ($f=35\%$) and a variable lattice parameter a (from 292 to 352 nm with a step of 10 nm).

The device testing was performed using a cryogenic probe station ($T=5$ K) equipped with cooled 50 Ω microwave probes. The LED current-voltage characteristic is shown in Fig. 3. A clear diode characteristic is observed even at low temperature, with a forward-bias (reverse-bias) threshold voltage around 2 V (-7 V), indicating very good electrical contacts.

Light emitted from the device was collected from the top using an external Cassegrain microscope objective (numerical aperture=0.4) and refocused to a single-mode fiber, providing a 1.8 μm diameter collection spot size. The EL spectrum at $I=1.25$ mA is shown in Fig. 4 (red line). A clear cavity mode is observed around 1329 nm, superposed

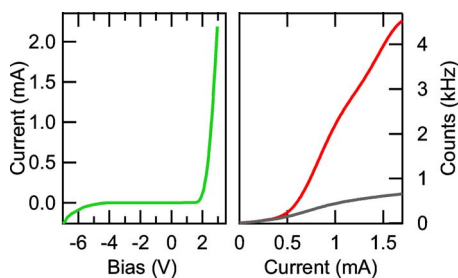


FIG. 3. (Color online) (left) IV characteristic of the device exhibiting diode operation. (Right) EL as a function of the injected current at the wavelength of the mode (red curve) and detuned from the mode (gray curve).

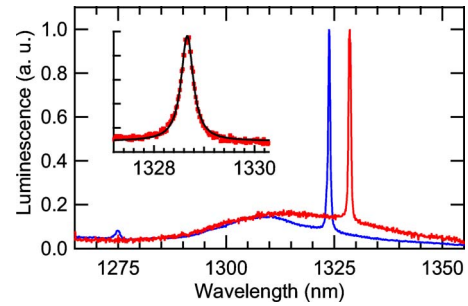


FIG. 4. (Color online) Photoluminescence (blue, 750 nm, 80 MHz) and EL (red, 2.3 V dc, 40 MHz) spectra of a PhC L3 cavity with lattice constant $a=341$ nm (mesa diameter: 10 μm). The quality factor of the mode is $Q\approx 4600$ (inset).

on a broad emission line corresponding to ground-state emission from the 10–20 QDs emitting within the collection area. The full width at half maximum (FWHM) of the mode peak is 0.29 nm (see inset of Fig. 4) corresponding to a quality factor $Q=4600$. The emission spectrum under optical pumping, measured on the same open-circuited device in a different microphotoluminescence setup, presents a very similar Q factor of ≈ 4000 (blue line). The small redshift (≈ 5 nm) observed in the EL spectrum is likely due to the different effects of adsorption of residual gas molecules in the two cryostats and/or to higher device temperature under electrical pumping. The total emission intensity in the mode was filtered with a tunable bandpass filter with a FWHM of 0.2 nm and measured with a fiber-coupled superconducting single photon detector (SSPD).⁹ The mode intensity is plotted as a function of injection current in Fig. 3 (right part, red line), along with the intensity measured when the filter is detuned by 15 nm from the mode (gray line). At low currents <0.5 mA, the two curves are superposed, and indeed no emission peak from the mode is observed in the spectra (not shown). The mode peak appears at currents larger than 0.5 mA and becomes much more intense than the QD ensemble. Despite the thresholdlike behavior of the light-current characteristics, we can rule out the occurrence of lasing since the threshold modal gain is much larger than the gain expected from the low-density QD ensemble, and the apparent threshold almost disappears when the temperature is increased to 77 K. Instead, the nonlinear light-current characteristics are due to the nonuniform current injection in the mesa: At low current carriers are injected only around the mesa edge (as confirmed by spatial imaging the EL), this effect being more evident at low temperatures due to the lower hole conductivity.

In order to provide a direct evidence of the spontaneous emission enhancement, we performed TR EL measurements on a cavity mode (on resonance) at 1319 nm with a quality factor $Q=1000$ and off resonance at 1310 nm. A constant bias voltage with a value $V_B=2.3$ V, below the threshold of the LED, is applied to the cavity. A transistor-transistor-Logic (TTL) signal is added on this constant voltage with a 40 MHz frequency and a 0.6 V amplitude, which results in the waveform shown in the inset of Fig. 5 and produces a periodic switching of the diode. The falling edge of this signal is used to measure the decay time of emission from the LED. The EL signal is spectrally filtered and coupled to the SSPD. The SSPD output pulse and the TTL trigger are sent to a correlation card to produce a histogram of photon arrival

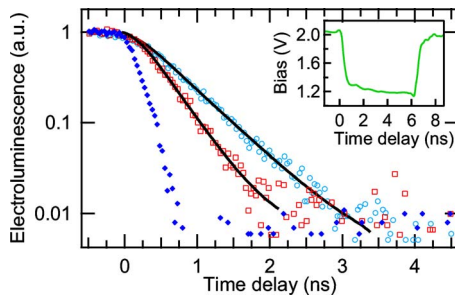


FIG. 5. (Color online) TR EL of the wetting layer (diamonds), mode (open squares), and detuned from the mode (open circles), under 40 MHz pulsed excitation. The electrical pulse waveform is shown in the inset. The measured average current is 1 mA.

times. The setup temporal resolution is determined by measuring the temporal decay (Fig. 5, blue diamonds) of emission from the wetting layer, whose lifetime is expected to be well below 100 ps. The measured decay time of ≈ 210 ps is mainly determined by the jitter of the SSPD and of the correlation card, as previously measured,¹⁰ which confirms that device parasitics are low and do not limit the dynamic behavior. The temporal decays of the cavity mode (red squares) and QD ensemble (blue dots) are shown in Fig. 5.

The time constants of both curves are calculated by fitting the experimental results using the convolution of a monoexponential curve with the time response of the experimental setup (fits are shown as lines in Fig. 5). Recombination lifetimes of $\tau_{\text{on}}=380$ ps and $\tau_{\text{off}}=580$ ps are obtained for the on-resonance and off-resonance emissions, respectively. Thus, an increase of the recombination rate by a factor of 1.5 is observed confirming a Purcell effect. We note that the off-resonance emission is faster than the typical exciton lifetime of similar QDs in bulk, which is around 1 ns.¹¹ EL decay times measured in similar LED structures without PhC cavities were also shorter, between 0.5 and 0.7 ns, depending on injection conditions, which could be due to the nonradiative effects and/or to emission from multiexcitons.¹⁰ We may write the measured recombination rate on resonance as $1/\tau_{\text{on}}=(1/2)(F_p^{\text{eff}}/\tau_0)+(1/\tau_{\text{NR}})+(1/\tau_{\text{leak}})$, where F_p is the effective Purcell factor taking into account any spatial and spectral mismatches between the emitter and the cavity,¹² τ_0 the radiative lifetime in the bulk, τ_{NR} and τ_{leak} the recombination times related to nonradiative recombination and radiative coupling to leakage modes, respectively,¹³ and the factor $\frac{1}{2}$ accounts for the fact the cavity mode is polarized while the emitter has two in-plane polarization components.¹⁴ As $1/\tau_{\text{off}}=(1/\tau_{\text{NR}})+(1/\tau_{\text{leak}})$, we derive $F_p^{\text{eff}}=2\tau_0[(1/\tau_{\text{on}})-(1/\tau_{\text{off}})]\approx 1/.5\pm 0.4$, assuming $\tau_0\approx 0.8\pm 0.2$ ns. Due to unoptimized QD-cavity spatial and spectral couplings, this value is much smaller than the theoretical value of the Purcell effect, for an ideal emitter spectrally narrower than the cavity and spatially aligned to the

cavity mode: $F_{p0}=3Q\lambda^3/4\pi^2n^3V_{\text{eff}}\approx 100$. By reducing the injection and/or the collection area, it should be possible to isolate the EL of single QDs and achieve higher Purcell factors.

In conclusion, we have demonstrated the enhancement of spontaneous emission dynamics in a PhC quantum dot LED. On the one hand, this opens the way to the fabrication of LEDs, diode lasers, and single-photon sources with a modulation speed and turn-on delay not limited by the free-space spontaneous emission time. On the other hand, the integration of electrical contacts with a coupled QD-cavity system allows the ultrafast electrical control of the coupling (for example, through the Stark tuning of the exciton energy), on a time scale shorter than the exciton coherence time. This will allow the coherent manipulation of excitonic and photonic qubits, a major step forward in the field of solid-state cavity quantum electrodynamics.

M. F. and L. B. contributed equally to this work. We are thankful to F. Römer and B. Witzigmann (ETHZ) for fruitful discussions, and we acknowledge funding from the Swiss SER through COST-P11 Project No. C05-70, the Swiss National Science Foundation through the “Professeur boursier” program, EU-FP6 IP “QAP” Contract No. 15848, the Network of Excellence “ePIXnet,” and the Italian MIUR-FIRB program.

¹E. M. Purcell, *Phys. Rev.* **69**, 681 (1946).

²J. M. Gérard, B. Sermage, B. Gayral, B. Legrand, E. Costard, and V. Thierry-Mieg, *Phys. Rev. Lett.* **81**, 1110 (1998).

³M. T. Hill, Y. S. Oei, B. Smalbrugge, Y. Zhu, T. De Vries, P. J. Van Veldhoven, F. W. M. Van Otten, T. J. Eijkemans, J. P. Turkiewicz, H. De Waardt, E. J. Geluk, S. H. Kwon, Y. H. Lee, R. Notzel, and M. K. Smit, *Nat. Photonics* **1**, 589 (2007).

⁴C. Bockler, S. Reitzenstein, C. Kistner, R. Debusmann, A. Loeffler, T. Kida, S. Hoffing, A. Forchel, L. Grenouillet, J. Claudon, and J. M. Gerard, *Appl. Phys. Lett.* **92**, 091107 (2008).

⁵F. Hofbauer, S. Grimminger, J. Angele, G. Bohm, R. Meyer, M. C. Amann, and J. J. Finley, *Appl. Phys. Lett.* **91**, 201111 (2007).

⁶H. G. Park, S. H. Kim, S. H. Kwon, Y. G. Ju, J. K. Yang, J. H. Baek, S. B. Kim, and Y. H. Lee, *Science* **05**, 1444 (2004).

⁷B. Alloing, C. Zinoni, V. Zwiller, L. H. Li, C. Monat, M. Gobet, G. Buchs, A. Fiore, E. Pelucchi, and E. Kapon, *Appl. Phys. Lett.* **86**, 101908 (2005).

⁸M. Bayer, T. L. Reinecke, F. Weidner, A. Larionov, A. McDonald, and A. Forchel, *Phys. Rev. Lett.* **86**, 3168 (2001).

⁹C. Zinoni, B. Alloing, L. H. Li, F. Marsili, A. Fiore, L. Lunghi, A. Gerardino, Yu. B. Vakhomina, K. V. Smirnov, and G. N. Gol'tsman, *Appl. Phys. Lett.* **91**, 031106 (2007).

¹⁰P. K. Bhattacharya, H.-J. Bühlmann, M. Hegems, and J. L. Staehli, *J. Appl. Phys.* **53**, 6391 (1982).

¹¹C. Zinoni, B. Alloing, C. Monat, V. Zwiller, L. H. Li, A. Fiore, L. Lunghi, A. Gerardino, H. de Riedmatten, H. Zbinden, and N. Gisin, *Appl. Phys. Lett.* **88**, 131102 (2006).

¹²J. M. Gérard, *Top. Appl. Phys.* **90**, 269 (2003).

¹³M. Schwab, H. Kurtze, T. Auer, T. Berstermann, M. Bayer, J. Wiersig, N. Baer, C. Gies, F. Jahnke, J. P. Reithmaier, A. Forchel, M. Benyoucef, and P. Michler, *Phys. Rev. B* **74**, 045323 (2006).

¹⁴I. C. Robin, R. André, A. Balocchi, S. Carayon, S. Moehl, J. M. Gérard, and L. Ferlazzo, *Appl. Phys. Lett.* **87**, 233114 (2005).